Effect of Winding Connection on Performance of a Six-Phase Switched Reluctance Machine

Xu Deng, Barrie Mecrow, *Member, IEEE*, Richard Martin, and Shady Gadoue

***Abstract*— In this paper, the effect of the stator winding connection on the performance of a six-phase Switched Reluctance Machine (SRM) is investigated. Five winding connection types are proposed for the machine. Finite element analyses (FEAs) of flux distribution and output torque are presented under single phase and multiphase excitation for each connection and the results are used to compare the average torque and torque ripple ratio characteristics and to develop understanding of the respective contributions of mutual inductance in torque development. Experimental tests on a six-phase conventional SRM verify the torque performance and mutual inductance effects of the different winding connections. An optimum winding configuration for a six-phase SRM is proposed.**

***Index Terms*— Current distortion, Mutual inductance, Stator windings, Switched Reluctance Machine (SRM), Torque ripple**

I. Introduction

Switched Reluctance Machines (SRMs) and their drive systems have the advantages of simple structure, low manufacturing cost, high system reliability, high efficiency and a wide speed range, and are contenders for electric vehicle traction drives [1-3]. In recent years they have also been developed for the aviation industry [4, 5].

However, torque development in SRMs is fundamentally prone to high ripple giving rise to vibration and acoustic noise, and this characteristic is a significant drawback [6]. The reduction of torque ripple is an active research topic and improvement strategies include machine design optimization [7-11] and advanced control techniques [12-15].

In the wake of power electronics development, increasing the phase number is a simple and generally accepted way to reduce torque ripple. In the last two decades, machines with higher phase numbers have become popular due to the potential for higher capacity, lower torque ripple, less phase current for a given power rating and better fault-tolerant ability compared with traditional machines [16, 17]. In addition, the choice of winding configuration in multi-phase machines has been investigated with a view to achieving a better torque performance and more flexible control [18, 19].

Xu Deng and Barrie Mecrow are with Electrical Power Group, School of Electrical and Electronic Engineering, Newcastle University, NE1 7RU, UK. (e-mail:xu.deng@ncl.ac.uk, barrie.mecrow@ncl.ac.uk).
Richard Martin is with Nidec SR Drives Ltd, East Part House, Otley Road, Harrogate, HG3 1PR, UK. (e-mail:richard.martin@nidec-motor.com)
Shady Gadoue is with the School of Engineering and Applied Science, Aston University, Birmingham, B4 7ET, UK. (e-mail:s.gadoue@aston.ac.uk)

The performance evaluation and the high performance control of SRMs require accurate flux linkage and torque information [12-15], both of which are nonlinear functions of phase current and rotor position. The flux linkage characteristic is usually obtained across the range of rotor positions and operating current values, and this information can then be used to facilitate advanced control techniques [20-22]. This approach is based on single-phase excitation, and can be accurate under multiphase excitation in situations where mutual inductance effects can be ignored.

As the phase number of an SRM increases, so too does the overlap between adjacent phases. This can give rise to considerable interaction between phases; in this case, the common analysis based on superposition of single phase, self-inductance characteristics is of limited application and it becomes necessary to consider mutual inductance effects. Winding connections for a 12/8 dual channel three-phase SRM have previously been investigated, and it has been suggested that connections giving rise to long flux paths exhibit better magnetic decoupling than those with short flux-paths [23].

Single-phase and two-phase excitation modes have been researched with a four-phase SRM [24, 25]; in this case, alternative winding connections can cause asymmetric instantaneous torque waveforms with high torque ripple. Although regulation of the asymmetric torque by increasing the chopping current was demonstrated in simulation, this is not an advanced control method and would be difficult to implement experimentally. It is clear that the mutual inductance cannot be ignored in multi-phase excitation mode unless a decoupling winding connection is employed [25].

More recently, a configuration has been proposed which enables a six-phase SRM to be driven with a three-phase full bridge inverter, thus reducing torque ripple without recourse to a non-standard converter [26]. Alternative winding connection types were investigated for this drive and a symmetric winding pattern was proposed whereby phase windings are unconventionally connected with opposing polarities, giving rise to significant phase interaction [27]. This drive has demonstrated high torque density and is proving to be a strong

candidate in electric vehicles applications [28].

In this paper, winding connections are investigated in a six-phase 12/10 SRM driven by an asymmetric half bridge converter. The distinction between reverse and forward series windings is introduced through Finite Element Analysis (FEA) under single-phase excitation. Furthermore, five different winding connection types are investigated through FEA, and comparisons are made on the bases of average torque and torque ripple. Flux density fields are analyzed at various rotor positions in order to illustrate variations of torque development between winding types. Finally, the analyses are verified through experimental tests on a 4kW prototype; measurements of instantaneous current and torque are presented for the different winding connections under single-phase and multi-phase excitation.

II. Winding Configurations for a Six-Phase SRM

In order to investigate output torque and mutual inductance effects, five winding connection types are proposed as illustrated in Fig. 1. Owing to the greater potential for phase interaction at higher phase numbers, the long/short flux path terminology is not appropriate and so a simplified classification is proposed here. Where the coil polarities of a given phase are magnetically in opposition, this is defined as N-S (North-South) connection type. Conversely, reinforcing phase coil polarities are defined as N-N (North-North) connection type.

For the six-phase 12/10 SRM under consideration there are five winding configurations which preserve an equal number of north and south polarity coils, as presented in Fig. 1. These comprise two N-N types (1 and 4) and three N-S types (2, 3, and 5).

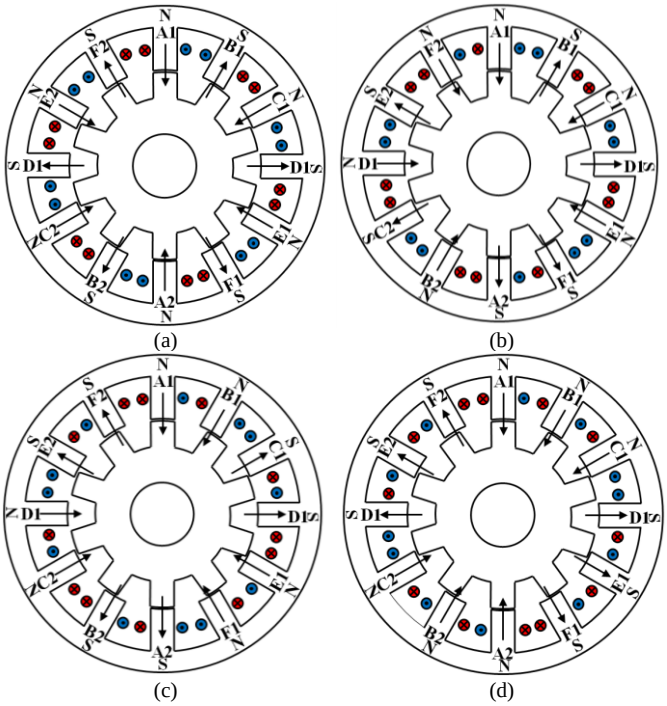

(a) (b) (c) (d)

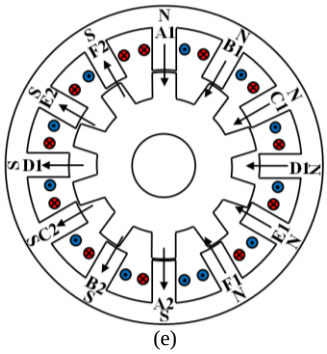

(e)

Fig. 1. The winding connections: (a) Type 1: NSNSNSNSNSNS (b) Type 2: NSNSNSSNSNSN (c) Type 3: NNSSNNSSNNSS (d) Type 4: NNNSSSNNNSSS (e) Type 5: NNNNNNSSSSSS

III. Finite Element Analysis

Fig. 2 shows the rotor and stator of the six-phase 12/10 SRM prototype, and Table I gives the design parameters for this machine.

(a)

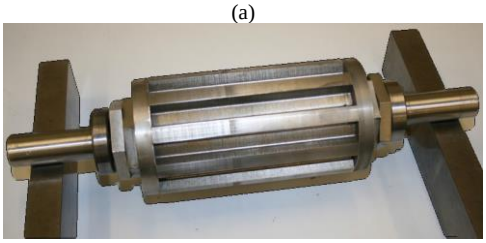

(b)

Fig. 2. Six-phase 12/10 SRM prototype: (a) wound stator (b) rotor

TABLE I
Design Parameters of the Six-Phase SRM prototype

Number of Stator Teeth	12
Number of Rotor Teeth	10
Axial Length	150.0mm
Stator Outer Diameter	150.0mm
Stator Inner Diameter	91.4mm
Stator Core-Back Depth	11.0mm
Stator Tooth Width	11.4mm
Airgap Length	0.3mm
Rotor Outside Diameter	90.8mm
Rotor Insider Diameter	36.0mm
Rotor Core back Depth	18.0mm
Rotor Tooth Width	11.4mm
Turns per Phase	100

A. *Single-Phase FEM analysis*

The six-phase 12/10 SRM under consideration has two coils per phase which may be connected in N-S or N-N type as previously defined. Single phase static FEA of the flux distributions arising from the two options are shown in Fig. 3.

As has previously been described [28], the N-S polarities of

the single-phase connection give rise to long flux paths via the full stator and rotor core (Fig. 3 (a)), whilst the N-N polarities of the single-phase connection give rise to shorter flux paths which link adjacent teeth (Fig. 3(b)).

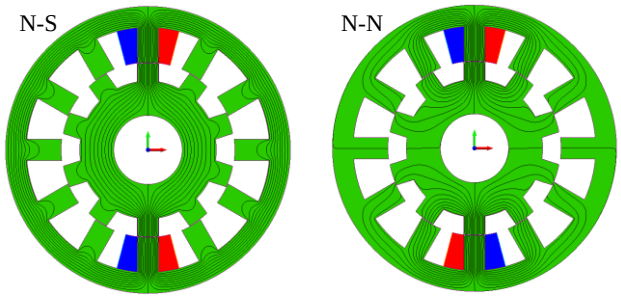

(a) (b)

Fig. 3. 2D FEA flux distribution under single phase excitation for: (a) N-N connection type (b) N-S connection type

Fig. 4 compares the phase flux linkages from 2D FEA for the N-N and N-S connections under single-phase excitation. As can be appreciated from inspection of Fig. 3, the single-phase N-S connection gives rise to large self-inductance and negligible mutual inductance, whereas the single-phase N-N connection gives rise to a slightly reduced self-inductance but considerable mutual inductance.

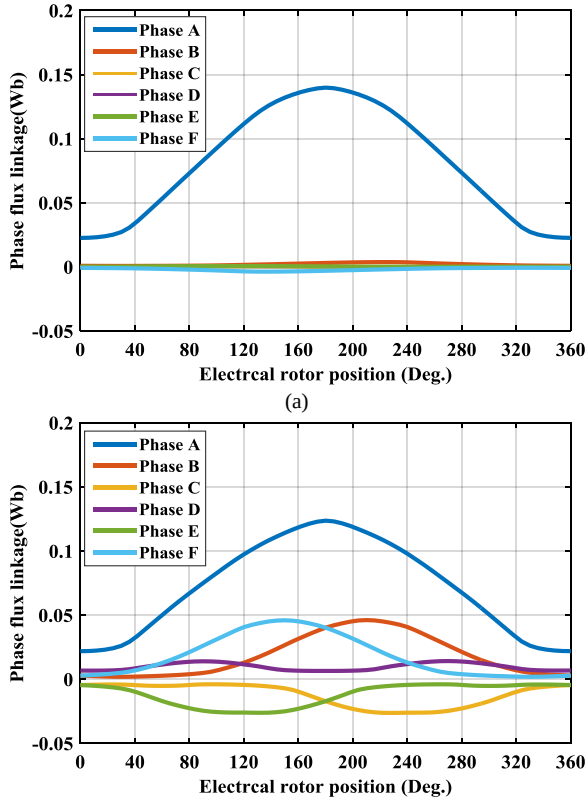

(a)

(b)

Fig. 4. Six phase flux linkages of N-N and N-S connection with single-phase excitation: (a) N-S connection type (b) N-N connection type

Fig. 5 presents instantaneous motoring torque waveforms under ideal current control from 2D FEA. The single phase torque for the forward and reverse series connections is compared with equivalent six-phase waveforms obtained by phase-shifted superposition. It is obvious that the N-S connection develops higher torque with both single phase excitation and six-phase superposition.

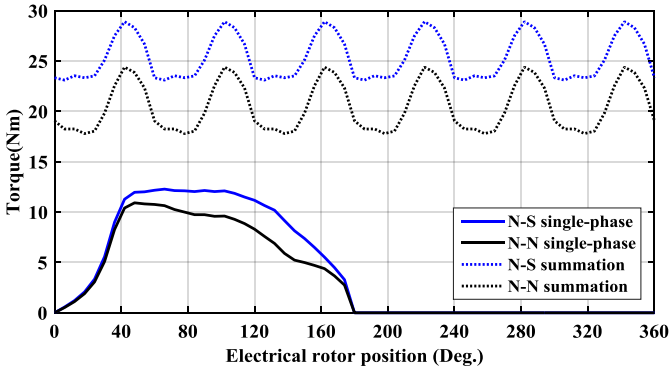

Fig. 5. Single phase torque output and six phase torque summation of N-S and N-N connection for a six-phase SRM

However, it should be noted that this approach neglects the torque contribution arising from the variation of mutual inductance in adjacent phases, which may be considerable in the N-S connection type as suggested by the flux linkage characteristics of Fig. 4.

B. Multi-phase FEM analysis

Fig. 6 presents instantaneous motoring torque waveforms under ideal current control with full six-phase excitation for the five winding connections, obtained from 2D FEA. Table II compares average torque and torque ripple ratio (TRR) of them.Type1 has the largest torque and type3 has the smallest torque ripple ratio in all the five configurations.

TABLE II
2D FEA AVERAGE TORQUE AND TRR COMPARISON

	Type1	Type2	Type3	Type4	Type5
Tav(Nm)	24.4	23.9	23.2	14.2	20.4
TRR(%)	27.2	29.2	16.7	243.0	58.8

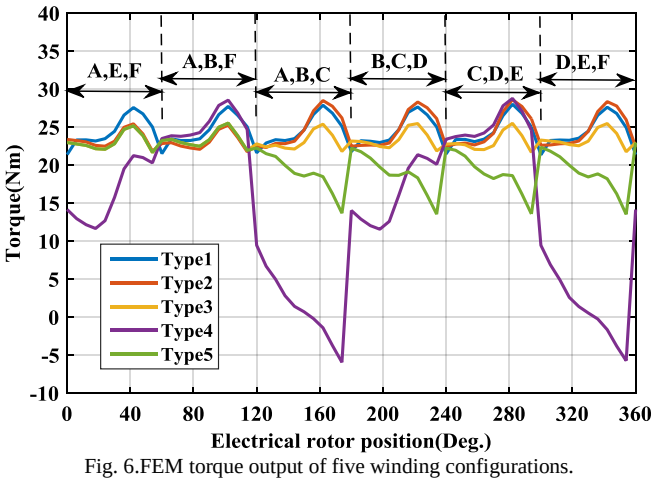

Fig. 6.FEM torque output of five winding configurations.

Picking out three typical conduction combinations, with which there are obvious instantaneous torque distinctions in Fig. 6, the torque relationships between these five types are summarized by (1).

$$\begin{cases} Type1 > Type2 = Type3 = Type5 > Type4, active \quad phases = A, E, F \\ Type1 = Type4 > Type2 = Type3 = Type5, active \quad phases = A, B, F \\ Type2 > Type1 > Type3 > Type5 > Type4, active \quad phases = A, B, C \end{cases} \quad (1)$$

Regardless of the presence of short or long flux paths arising from a given winding connection, there are two fundamental factors act to reduce the mean torque and increase the torque ripple: 1) saturation in the stator core back; and 2) unwanted flux giving rise to negative torque in a particular phase.

Negative torque production is unavoidable to some extent in all of the winding connections under consideration owing to the phase overlap and prevalence of at least some mutual coupling. However, the impact of stator core back saturation can readily be illustrated, to which end the FEA described at the start of section B is repeated here with the stator core back depth increased sufficiently to prevent performance limitation in any of the winding connection types.

The results are illustrated in Fig. 7 which shows that, in the absence of stator core back saturation, types 1-3 and 5 develop very similar torque waveforms with type 4 being the notably inferior exception. Furthermore, comparison with Fig. 6 suggests that, in the absence of stator core back saturation, the torque characteristics converge on that of type 1. Thus, with the actual stator core back limitation, it is obvious that type 1 is preferable in that it develops greater torque, and that types 4 and 5 are clearly inferior.

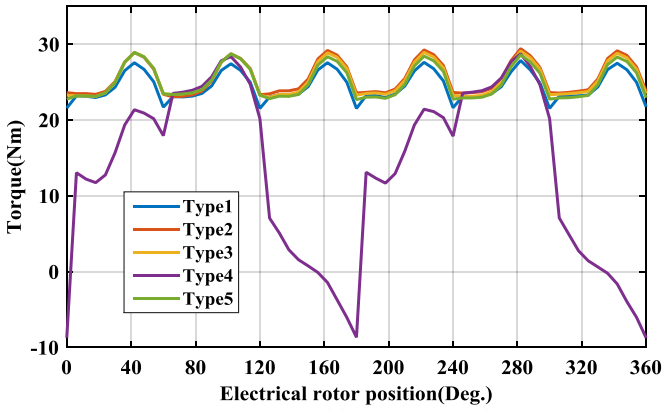

Fig. 7. FEM torque output of five winding configurations.

In order to further explain the reasons causing different instantaneous torques in Fig. 6, flux linkage distribution of three typical conduction combinations are observed.

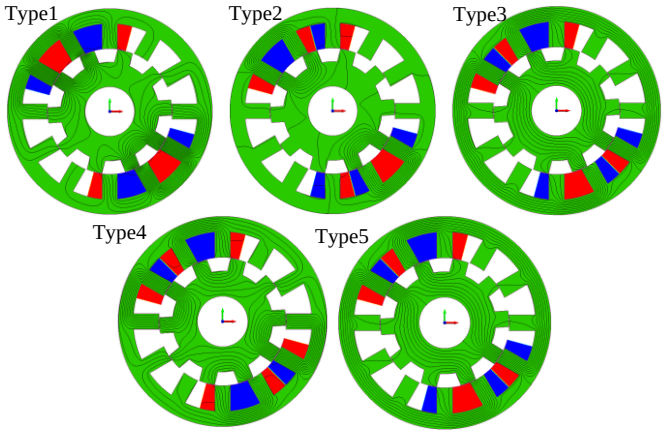

Fig. 8. Comparison of flux distribution when phase A,E,F are active.

When phases A, E and F are conducting as shown in Fig. 8, the majority of the torque is produced by phases A and E whilst phase F is nearly aligned.

Producing the largest instantaneous torque, type1 has six short flux-paths, and the majority of flux goes through the proximate four teeth and a quarter of the stator and rotor cores. Producing second largest torque, the majority of the flux of type2 comprises only two short paths. Types 3 and 5 have the same flux distribution, comprising two long flux-paths with the majority of flux passing through the full stator and rotor core, and producing the same instantaneous torque as type2. Type4 has four short flux-paths, but unlike the other four types it has less flux in the conducting phases than the non-conducting phases and therefore produces more negative torque at this position.

In addition, it is clear that, by comparison with type1, more energy is stored in the stator core back in types 2, 3 and 5. Furthermore, type1 exhibits more energy in the teeth which is indicative of a higher torque contribution.

When, phases A, B and F are conducting as shown in Fig. 9, the majority of the torque is produced by phases A and B whilst phase F is nearly aligned.

Type1 keeps six short flux-paths and type4 has two short and two long flux-paths, and they produce the same and the largest torque at this position. Types 3 and 5 have the same flux distribution again, and produce less torque than types 1 and 4. Having two short flux-paths, type2 has the same torque as types 3 and 5.

Furthermore, compared with other three types, types 1 and 4 have less flux density in stator core back, exhibiting more energy in the teeth, which is indicative of a higher torque contribution.

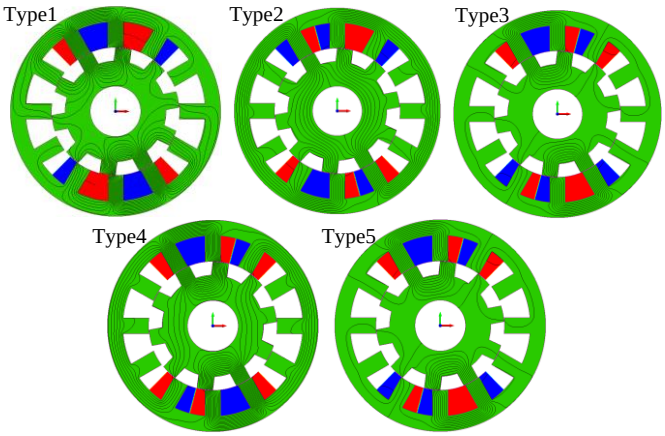

Fig. 9. Comparison of flux distribution when phase A,B,F are active.

When phases A, B and C are conducting as shown in Fig. 10, the majority of the torque is produced by phases B and C whilst phase A is nearly aligned.

Type2 in Fig. 10 has similar flux distribution to type4 in Fig. 9. All the flux links the three conducting phases, thus no extra negative torque is produced, which results in type2 developing the largest torque in Fig. 10. With only short flux-path in type1 and only long flux-paths in type3, these develop the second and third greatest torque respectively at this position. Type4 develops a reduced torque at this position owing to the negative contribution from mutual flux linking inactive phases with

reducing inductance. Unlike the previous two positions, the flux distribution of type5 is not exactly the same as type3. A higher flux density appears in stator core back and lower flux density appears in conducting teeth of type5, which reduces instantaneous torque.

In conclusion, the majority of flux linkage distributes in conducting teeth in types 1, 2, 3 and 5 at any rotor position. Slight flux linkage appears in non-conducting teeth of types 1, 2, 3 and 5 gives rise to negative torque. The different flux density in non-conducting teeth primarily depends on polarities arrangement and is affected by stator core back saturation.

However, the situation of types 4 is different with other four types. At some rotor position, non-conducting teeth of type4 has pronounced higher flux density compared with types 1, 2, 3 and 5. This unexpected flux distribution is even worse when adjacent three conducting phases have the same polarity (Type4 in Fig. 10).

IV. Mutual Inductance in a Six-Phase SRM

Under idealized current excitation with 180° conduction, up to three phases may be energized at any instant. This situation can be summarized by referring to the out-going phase, intermediate phase and in-coming phase as illustrated in Fig. 11.

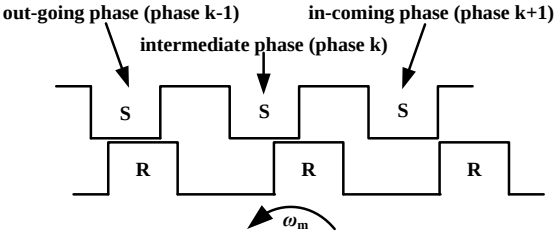

Fig. 11. Definition of three conducting phases

For a six-phase SRM, phase flux linkages can be expressed:

$$\begin{bmatrix}\psi_A\\ \psi_B\\ \psi_C\\ \psi_D\\ \psi_E\\ \psi_F\end{bmatrix}=\begin{bmatrix}L_A & M_{AB} & M_{AC} & M_{AD} & M_{AE} & M_{AF}\\ M_{AB} & L_B & M_{BC} & M_{BD} & M_{BE} & M_{BF}\\ M_{AC} & M_{BC} & L_C & M_{CD} & M_{CE} & M_{CF}\\ M_{AD} & M_{BD} & M_{CD} & L_D & M_{DE} & M_{DF}\\ M_{AE} & M_{BE} & M_{CE} & M_{DE} & L_E & M_{EF}\\ M_{AF} & M_{BF} & M_{CF} & M_{DF} & M_{EF} & L_F\end{bmatrix}\times\begin{bmatrix}i_A\\ i_B\\ i_C\\ i_D\\ i_E\\ i_F\end{bmatrix} \quad (2)$$

Mutual inductances between non-conducting phases may be ignored, giving:

$$\begin{bmatrix}\psi_{k-1}\\ \psi_k\\ \psi_{k+1}\end{bmatrix}=\begin{bmatrix}L_{k-1} & M_{(k-1)k} & M_{(k-1)(k+1)}\\ M_{(k-1)k} & L_k & M_{k(k+1)}\\ M_{(k-1)(k+1)} & M_{k(k+1)} & L_{k+1}\end{bmatrix}\times\begin{bmatrix}i_{k-1}\\ i_k\\ i_{k+1}\end{bmatrix} \quad (3)$$

Where $M_{(k-1)k}$, $M_{(k-1)(k+1)}$ and $M_{k(k+1)}$ are mutual inductances between three adjacent, conducting phases. Assuming fixed phase current (I) in each phase, the mutual inductances are given:

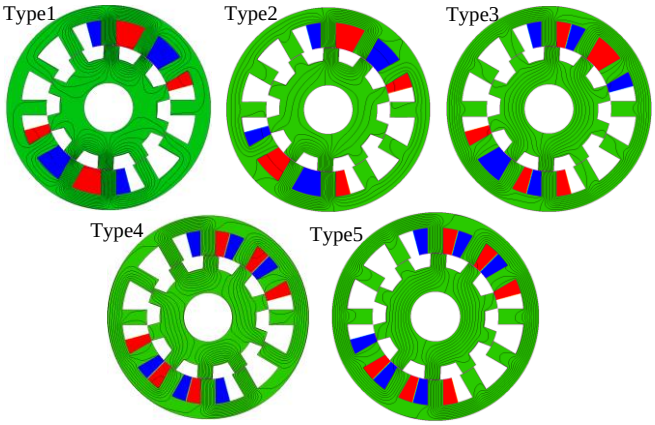

Fig. 10. Comparison of flux distribution when phase A,B,C are active.

$$M_{(k-1)k}=\frac{I(L_{k-1}-L_k-L_{k+1})-(\psi_{k-1}-\psi_k-\psi_{k+1})}{2I} \quad (4)$$

$$M_{(k-1)(k+1)}=\frac{(\psi_{k-1}-\psi_k+\psi_{k+1})-I(L_{k-1}-L_k+L_{k+1})}{2I} \quad (5)$$

$$M_{k(k+1)}=\frac{(\psi_{k-1}+\psi_k-\psi_{k+1})-I(L_{k-1}+L_k-L_{k+1})}{2I} \quad (6)$$

Mutual inductance of inactive phase can be calculated by:

$$M=\frac{\psi_m}{I} \quad (7)$$

The variation of mutual inductance in each phase across an electrical cycle was obtained from 2D FEA with phase current I = 15A for winding connection types 1, 2, and 3 (4 and 5 being clearly inferior as described in section III). The results are shown in Fig. 12.

As expected, types 1 to 3 have very similar and small mutual inductance value during the active period, all being between -1mH to 1mH. However, the mutual inductance in the inactive period has clear distinctions. Phase mutual inductances are close to 3mH or -2mH for type1 in the inactive period, whilst type3 exhibits a maximum of 1.6mH as the maximum value; only three phases have obvious mutual inductance in type2 with a maximum value less than 1.8mH.

Combining these observations with the output torque results of Fig. 6, is clear that the asymmetric mutual inductances result in a larger torque ripple in type2. In addition, the large positive mutual inductance after the active period could delay the demagnetization time at low speed and cause current distortion in a real-time system especially at high speed.

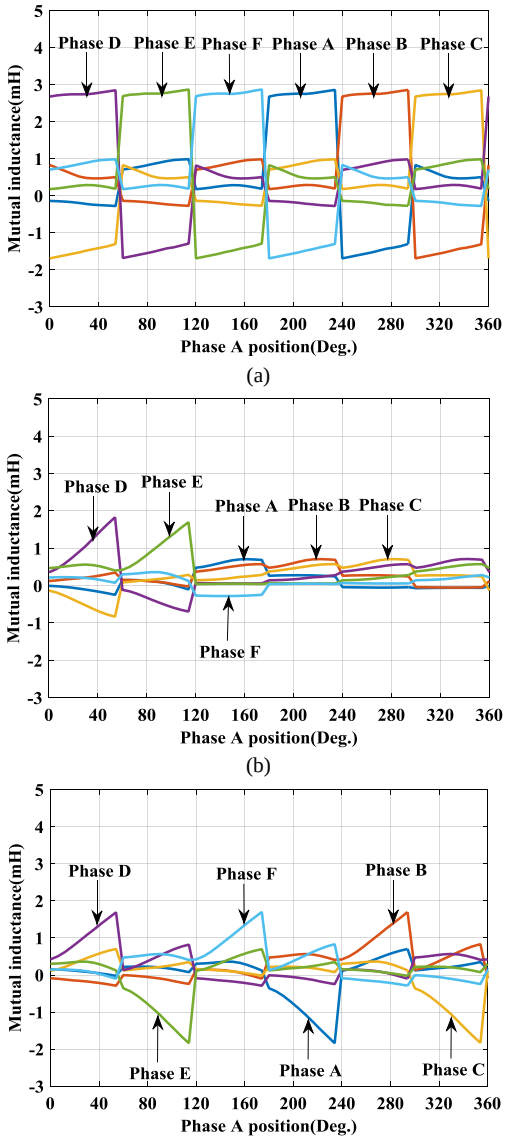

Fig. 12. Six phase mutual inductances of three different winding connection types excited by 180° 15A square wave current: (a) type1 (b) type2 (c) type3

V. Experimental Verification

In order to compare the characteristics of the five winding connection types, and verify the simulation results and conclusions of the preceding sections, experimental work was undertaken. The test rig consists of: the prototype six-phase SRM; a Permanent Magnet Synchronous Machine (PMSM) acting as a load; and a six-phase asymmetric half bridge converter and controller as shown in Fig. 13.

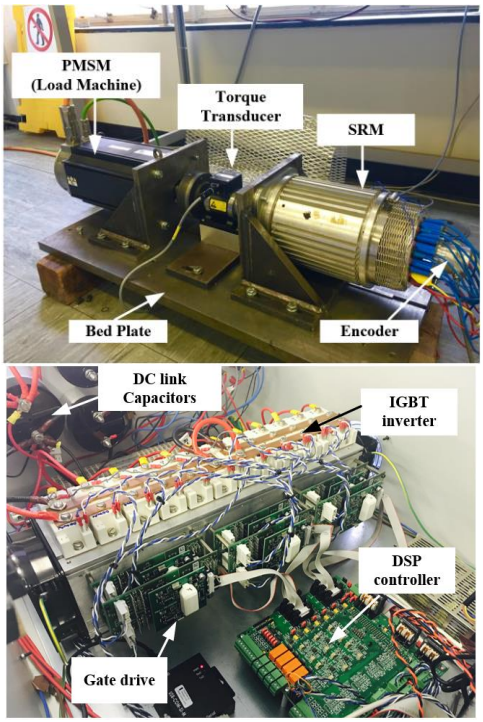

Fig. 13. Photos of test rig.

A. Single-phase excitation experimental results

Table III compares single-phase excitation torque measurement with the predictions of FEA. In this test, the conduction width is 180º, the advance angle is 0º, the current reference is 15A, the DC link voltage is 100V, the switching frequency is 10kHz, and the rotational speed is 200r/min. The experimental results verify that the N-S connection can produce greater mean torque from single phase excitation. Variation between FEA and measured results is mainly due to the 2D FEA approach which neglects end leakage and thus over predicts torque.

TABLE III
SINGLE PHASE AVERAGE TORQUE COMPARISON BETWEEN FEA AND EXPERIMENTAL TEST

	N-S(FEA)	N-S(Test)	N-N(FEA)	N-N(Test)
T_{av}(Nm)	3.75	3.55	3.30	3.15

B. Multi-phase excitation experimental results

1) Current control mode

Fig. 14 presents the instantaneous torque and phase A current waveforms for the five different winding configurations. The same current reference values are applied to all six phase windings, and all the other parameters are the same as those for single-phase excitation.

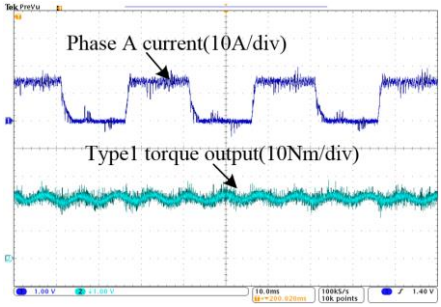

(a)

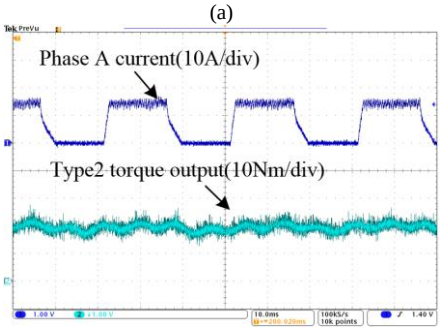

(b)

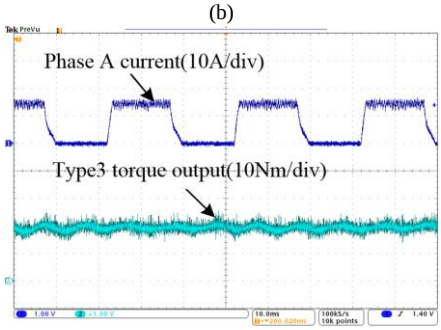

(c)

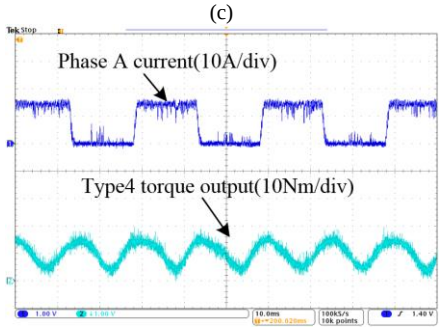

(d)

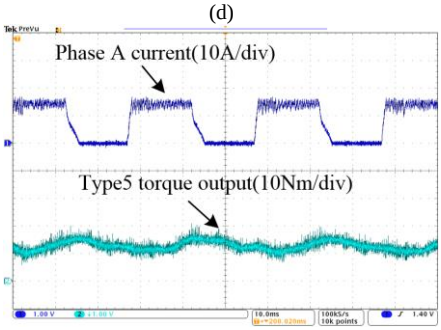

(e)

Fig. 14. Torque output waveforms of multi-phase excitation tests at 200r/min: (a) type1 (b) type2 (c) type3 (d) type4 (e) type5

TABLE IV
EXPERIMENTAL AVERAGE TORQUE AND TRR COMPARISON

	Type1	Type2	Type3	Type4	Type5
Tav(Nm)	22.6	20.8	19.7	10.2	12.5
TRR(%)	29.2	36.7	25.6	126.3	52.1

The measurements show that type1 has the largest average torque, and type3 has the smallest torque ripple as predicted by FEA. It is clear that the phase current of type1 in Fig. 14(a) exhibits some noise which arises from the presence of a high level of mutual coupling throughout this period as observed in the analysis of Fig. 12(a).

In order to illustrate the effects of mutual inductance, the full six phase current waveforms of type3 are shown in Fig. 15. With reference to the reducing current at the point of commutation, two different characteristics can be observed: phases A, C and E (encircled red) and phases B, D and F (encircled black). This compares well with the binary phase groupings of mutual inductance observed in Fig. 12(c).

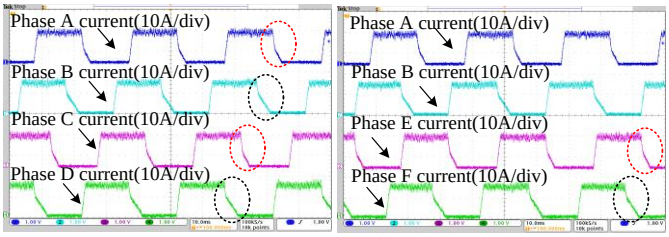

Fig. 15. Six phase current waveforms of type3 by current control

Fig. 16 presents the average output torque and torque ripple with excitation current varying from 0 to 20A. Types 1 to 3 exhibit greater average output torque (Fig. 16(a)), and type2 exhibits the smallest torque ripple (Fig. 16(b)) over the range of current.

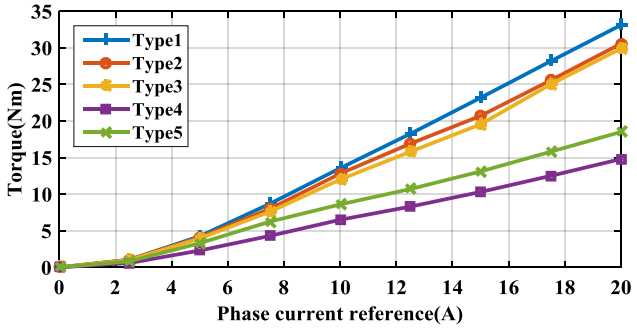

(a)

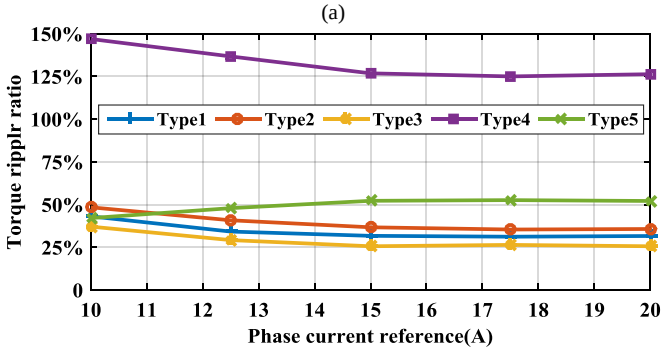

(b)

Fig. 16. Average output torque and torque ripple ratio with current control: (a)average torque (b) torque ripple ratio

2) Voltage control mode

In order to further investigate the mutual inductance effect on torque performance at higher speed, the Angle Position Control

(APC) method is employed. In this test, current is not controlled by chopping and is now a function of the applied voltage and machine impedance. Hence this test brings further insight into the effects mutual inductance. Fig. 17 shows measured phase currents for multi-phase excitation under voltage control at 800r/min. The conduction period is 140º, and the advance angle is 10º. Again, more pronounced current distortion is evidence of greater mutual coupling in type1 by comparison with types 2 and 3.

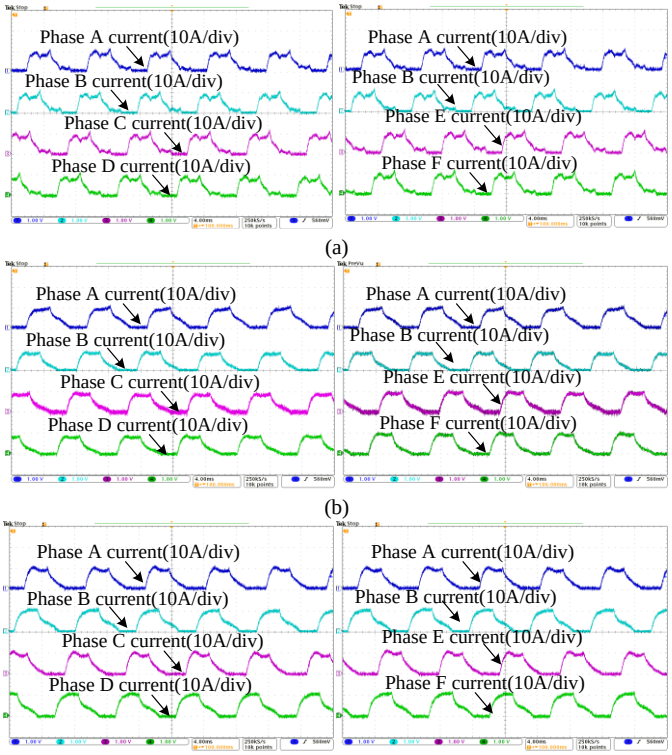

Fig. 17. Six phase current waveforms of multi-phase excitation tests at 800r/min: (a) type1 (b) type2 (c) type3

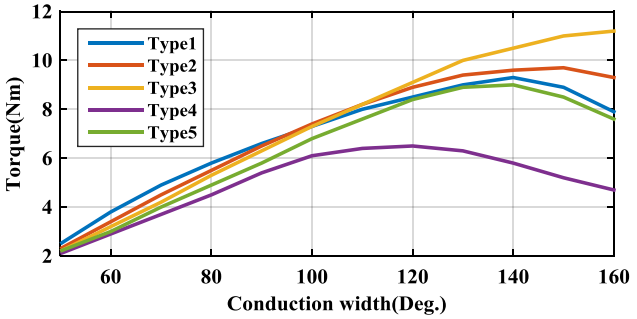

Fig. 18. Experimental results of average torque with voltage control.

Fig. 18 shows experimental results for average output torque with different conduction angles for the five winding connection types at 800r/min. Types 2 and 3 are generally superior above 120 degrees of conduction owing to better decoupling which means more current coincides with increasing inductance (more torque) and the shorter tail on the current waveform gives a reduced negative torque contribution, as shown in Fig. 17. Type 1 exhibits greater torque at lower conduction angles, but at higher angles the current distortion is considerable as shown in Fig. 17(a), and this compromises the torque output.

VI. Conclusion

In this paper, five different winding connection types for a six-phase SRM are investigated and compared on the bases of torque performance and mutual inductance effects. The predictions of FEA and the results of experimental tests including single-phase excitation and multi-phase excitation are examined and compared. Owing to the considerable mutual inductances in type1, phase currents are more difficult to control and exhibit serious distortion at high speed; therefore, although type1 has the biggest average torque at low speed, it not an ideal winding connection type for the six-phase SRM. Types 4 and 5 have inferior performances throughout the whole speed range, they are obviously not suitable for the six-phase SRM. The proposed types 2 and 3 have reasonable average torque and less mutual inductance throughout the whole speed range. However, type3 has large torque ripple due to its asymmetric connection type. Consequently type2 is selected to be the optimum winding connection type for the six-phase SRM prototype.

References

[1] R. Madhavan and B. G. Fernandes, "Axial Flux Segmented SRM With a Higher Number of Rotor Segments for Electric Vehicles," *IEEE Transactions on Energy Conversion*, vol. 28, pp. 203-213, 2013.

[2] K. M. Rahman, B. Fahimi, G. Suresh, A. V. Rajarathnam, and M. Ehsani, "Advantages of switched reluctance motor applications to EV and HEV: design and control issues," *IEEE Transactions on Industry Applications*, vol. 36, pp. 111-121, 2000.

[3] B. Bilgin, A. Emadi, and M. Krishnamurthy, "Comprehensive Evaluation of the Dynamic Performance of a 6/10 SRM for Traction Application in PHEVs," *IEEE Transactions on Industrial Electronics*, vol. 60, pp. 2564-2575, 2013.

[4] M. Krishnamurthy, C. S. Edrington, A. Emadi, P. Asadi, M. Ehsani, and B. Fahimi, "Making the case for applications of switched reluctance motor technology in automotive products," *IEEE Transactions on Power Electronics*, vol. 21, pp. 659-675, 2006.

[5] Y. Sozer, I. Husain, and D. A. Torrey, "Guidance in Selecting Advanced Control Techniques for Switched Reluctance Machine Drives in Emerging Applications," *IEEE Transactions on Industry Applications*, vol. 51, pp. 4505-4514, 2015.

[6] I. Husain, "Minimization of torque ripple in SRM drives," *IEEE Transactions on Industrial Electronics*, vol. 49, pp. 28-39, 2002.

[7] L. Guangjin, J. Ojeda, S. Hlioui, E. Hoang, M. Lecrivain, and M. Gabsi, "Modification in Rotor Pole Geometry of Mutually Coupled Switched Reluctance Machine for Torque Ripple Mitigating," *IEEE Transactions on Magnetics*, vol. 48, pp. 2025-2034, 2012.

[8] H. Eskandari and M. Mirsalim, "An Improved 9/12 Two-Phase E-Core Switched Reluctance Machine," *IEEE Transactions on Energy Conversion*, vol. 28, pp. 951-958, 2013.

[9] C. Yong Kwon, Y. Hee Sung, and K. Chang Seop, "Pole-Shape Optimization of a Switched-Reluctance Motor for Torque Ripple Reduction," *IEEE Transactions on Magnetics*, vol. 43, pp. 1797-1800, 2007.

[10] C. Ma and L. Qu, "Multiobjective Optimization of Switched Reluctance Motors Based on Design of Experiments and Particle Swarm Optimization," *IEEE Transactions on Energy Conversion*, vol. 30, pp. 1144-1153, 2015.

[11] N. K. Sheth and K. R. Rajagopal, "Optimum pole arcs for a switched reluctance motor for higher torque with reduced ripple," *IEEE Transactions on Magnetics*, vol. 39, pp. 3214-3216, 2003.

[12] P. Pillay, M. Ahmed, and M. Samudio, "Modeling and performance of a SRM drive with improved ride-through capability," *IEEE Transactions on Energy Conversion*, vol. 16, pp. 165-173, 2001.
[13] M. Takiguchi, H. Sugimoto, N. Kurihara, and A. Chiba, "Acoustic Noise and Vibration Reduction of SRM by Elimination of Third Harmonic Component in Sum of Radial Forces," *IEEE Transactions on Energy Conversion*, vol. 30, pp. 883-891, 2015.
[14] Y. Jin, B. Bilgin, and A. Emadi, "An Offline Torque Sharing Function for Torque Ripple Reduction in Switched Reluctance Motor Drives," *IEEE Transactions on Energy Conversion*, vol. 30, pp. 726-735, 2015.
[15] S. K. Sahoo, S. K. Panda, and J. X. Xu, "Iterative learning-based high-performance current controller for switched reluctance motors," *IEEE Transactions on Energy Conversion*, vol. 19, pp. 491-498, 2004.
[16] J. A. Haylock, B. C. Mecrow, A. G. Jack, and D. J. Atkinson, "Operation of a fault tolerant PM drive for an aerospace fuel pump application," *IEE Proceedings on Electric Power Applications*, vol. 145, pp. 441-448, 1998.
[17] X. Chen, J. Wang, V. I. Patel, and P. Lazari, "A Nine-Phase 18-Slot 14-Pole Interior Permanent Magnet Machine with Low Space Harmonics for Electric Vehicle Applications," *IEEE Transactions on Energy Conversion*, vol. PP, pp. 1-1, 2016.
[18] A. S. Abdel-Khalik, A. S. Morsy, S. Ahmed, and A. M. Massoud, "Effect of Stator Winding Connection on Performance of Five-Phase Induction Machines," *IEEE Transactions on Industrial Electronics*, vol. 61, pp. 3-19, 2014.
[19] F. J. T. E. Ferreira and A. T. d. Almeida, "Method for in-field evaluation of the stator winding connection of three-phase induction motors to maximize efficiency and power factor," *IEEE Transactions on Energy Conversion*, vol. 21, pp. 370-379, 2006.
[20] Z. Jinhui and A. V. Radun, "A New Method to Measure the Switched Reluctance Motor's Flux," *IEEE Transactions on Industry Applications*, vol. 42, pp. 1171-1176, 2006.
[21] P. Debiprasad and V. Ramanarayanan, "Mutual Coupling and Its Effect on Steady-State Performance and Position Estimation of Even and Odd Number Phase Switched Reluctance Motor Drive," *IEEE Transactions on Magnetics*, vol. 43, pp. 3445-3456, 2007.
[22] N. Radimov, N. Ben-Hail, and R. Rabinovici, "Inductance measurements in switched reluctance machines," *IEEE Transactions on Magnetics*, vol. 41, pp. 1296-1299, 2005.
[23] W. Ding, D. Liang, and Z. Luo, "A comparative study of performances for a dual channel switched reluctance machine with different winding connections," in *International Conference on Electrical Machines and Systems, 2011*, 2011, pp. 1-5.
[24] Q. Bingni, S. Jiancheng, L. Tao, and Z. Hongda, "Mutual coupling and its effect on torque waveform of even number phase switched reluctance motor," in *International Conference on Electrical Machines and Systems*, 2008, pp. 3405-3410.
[25] G.J.Li, J. Ojeda, E. Hoang, M. Lecrivain, and M. Gabsi, "Comparative Studies Between Classical and Mutually Coupled Switched Reluctance Motors Using Thermal-Electromagnetic Analysis for Driving Cycles," *IEEE Transactions on Magnetics*, vol. 47, pp. 839-847, 2011.
[26] J. D. Widmer, B. C. Mecrow, C. M. Spargo, R. Martin, and T. Celik, "Use of a 3 phase full bridge converter to drive a 6 phase switched reluctance machine," in *6th IET International Conference on Power Electronics, Machines and Drives* 2012, pp. 1-6.
[27] J. D. Widmer, R. Martin, C. M. Spargo, B. C. Mecrow, and T. Celik, "Winding configurations for a six phase switched reluctance machine," in *XXth International Conference on Electrical Machines (ICEM)* 2012, pp. 532-538.
[28] R. Martin, J. D. Widmer, B. Mecrow, M. Kimiabeigi, A. Mebarki, and N. L. Brown, "Electromagnetic Considerations for a Six-Phase Switched Reluctance Motor Driven by a Three-Phase Inverter," *IEEE Transactions on Industry Applications*, vol. PP, pp. 1-1, 2016.